AD-A277 604

TATION PAGE

Form Approved OMB No 0704-0178

1 DATE	3. REPORT TYPE AND DATES COVERED
	FINAL/01 JUN 92 TO 31 AUG 93

4. TITLE AND SUBTITLE
BISTATIC CLUTTER RCS SIMULATION USING SCALE
MODEL SURVACES WITH TWO WCALE ROUGHNESS (U)

5. FUNDING NUMBERS
61102F
2304/BS
F49620-92-J-0212

6. AUTHOR(S)
Professor Zoltan Fried

7. PERFORMING ORGANIZATION NAME(S) AND ADDRESS(ES)
Univ of Massachusetts
Dept of Physics
One University Avenue
Lowell, MA 01854

8. PERFORMING ORGANIZATION REPORT NUMBER

AFOSR-TR· 94 0091

DTIC
ELECTE
MAR 28 1994
S F D

9. SPONSORING/MONITORING AGENCY NAME(S) AND ADDRESS(ES)
AFOSR/NM
110 DUNCAN AVE, SUITE B115
BOLLING AFB DC 20332-0001

10. SPONSORING/MONITORING AGENCY REPORT NUMBER
F49620-92-J-0212

11. SUPPLEMENTARY NOTES

12a. DISTRIBUTION/AVAILABILITY STATEMENT

Approved for public release;
distribution unlimited.

APPROVED FOR PUBLIC RELEASE: DISTRIBUTION IS UNLIMITED

12b. DISTRIBUTION CODE
UL

13. ABSTRACT *(Maximum 200 words)*

Bistatic scattering cross section measurements of CO_2 laser radiation from slightly roughened metallic surfaces were made and compared to the predictions of the Rice theory. Co-pol and cross pol measurements were performed both in and out of the plane of incidence. The incident radiation was linearly polarized in either the H or V configuration, perpendicular and parallel to the plane of incidence, respectively. For each state of incident polarization the scattered polarization was analyzed along two directions, perpendicular, (HH) and (HV), and Parallel, (HV) and (VV), to the scattering plane. The Rice theory predicts the polarization dependent scattering cross section from a roughened surface with small scale roughness.

14. SUBJECT TERMS

15. NUMBER OF PAGES
42

16. PRICE CODE

17. SECURITY CLASSIFICATION OF REPORT	18. SECURITY CLASSIFICATION OF THIS PAGE	19. SECURITY CLASSIFICATION OF ABSTRACT	20. LIMITATION OF ABSTRACT
UNCLASSIFIED	UNCLASSIFIED	UNCLASSIFIED	SAR(SAME AS REPORT)

DTIC QUALITY INSPECTED 1

Final Technical Report

October 29, 1993

Bistatic Clutter RCS Simulation Using Scale Model Surfaces with Two Scale Roughness

DEPARTMENT OF PHYSICS

UNIVERSITY OF MASSACHUSETTS, LOWELL
Lowell, Massachusetts 01854

Z. Fried, J. Waldman, G. Phillips and C. Laramee

94-09432

94 3 25 122

TABLE OF CONTENTS

Accesion For	
NTIS CRA&I	☑
DTIC TAB	☐
Unannounced	☐
Justification	
By	
Distribution /	
Availability Codes	
Dist	Avail and / or Special
A-1	

Abstract

Bistatic scattering cross section measurements of CO_2 laser radiation from slightly roughened metallic surfaces were made and compared to the predictions of the Rice theory. Co-pol and cross pol measurements were performed both in and out of the plane of incidence. The incident radiation was linearly polarized in either the H or V configuration, perpendicular and parallel to the plane of incidence, respectively. For each state of incident polarization the scattered polarization was analyzed along two directions, perpendicular, (HH) and (HV), and parallel. (HV) and (VV), to the scattering plane. The Rice theory predicts the polarization dependent scattering cross section from a roughened surface with small scale roughness. Small scale roughness is defined in terms of $\frac{h}{\lambda}$, where h is the rms value of the randomly distributed surface depths and λ the wavelength of the incident radiation. A roughened surface with $\frac{h}{\lambda} < \frac{1}{2\pi}$ is considered to be small scale. The aluminum surfaces that were prepared for targets all satisfied the criteria for small scale roughness. The rms depth was obtained from specular reflection data which was fitted to the Davies formula, and the average slopes were obtained from profilometric traces.

I INTRODUCTION

In the branch of macroscopic electromagnetic physics dealing with scattering from rough surfaces, scattering from surfaces with small scale roughness commands special attention. The primary reason for this is that the problem can be treated analytically provided that certain criteria pertaining to the rms depth and correlation length are satisfied.

Historically, the acoustic version of this problem, the scattering of sound waves from surfaces with small scale roughness, was solved by Rayleigh[1]. More than a half of a century later, Rice[2][3] adopted Rayleigh's computational technique to the electromagnetic case. The electromagnetic case differs significantly from the acoustic problem in that the electromagnetic waves are vector waves. Nevertheless, in a first order perturbation treatment of the problem, the polarization state scattering matrix elements are independent of the exact nature of the rough surface.

As an example, for a perfectly conducting surface the scattering matrix elements are given by :

$$\alpha_{HH} = -\cos(\phi_s) \tag{1}$$

$$\alpha_{VH} = -\sin(\phi_s) / \cos(\theta_s) \tag{2}$$

$$\alpha_{HV} = \sin(\phi_s) / \cos(\theta_s) \tag{3}$$

$$\alpha_{VV} = \frac{\sin(\theta_i)\sin(\theta_s) - \cos(\phi_s)}{\cos(\theta_i)\cos(\theta_s)} \tag{4}$$

where H stands for horizontal linear polarization state and V designates vertical polarization.

From left to right the first label stands for the polarization of the scattered amplitude and the second label corresponds to the incident state polarization. ϕ denotes the azimuthal angle, and θ the polar angle. Subscripts i and s attached to ϕ and θ are abbreviations for incident and scattered, respectively. Horizontal polarization state refers to the electric field vector being perpendicular to either the incident or scattered plane, and by vertical polarization state we mean that the electric field vector is either in the incident or scattering plane. If the rough surface satisfies some fairly general conditions, which will be elaborated on in our subsequent discussion, the polarization state dependent cross section ratios depend solely on the ratios of the squares of the respective matrix element given in equations (1.) - (4.). Thus, to first order in perturbation theory

$$\frac{\sigma_{HH}(\theta_s,\phi_s)}{\sigma_{VV}(\theta_s,\phi_s)} = \frac{\cos^2(\phi_s)\cos^2(\theta_i)\cos^2(\theta_s)}{(\sin(\theta_i)\sin(\theta_s)-\cos^2(\phi_s))^2} \tag{5}$$

where σ stands for the scattering cross-section.

Similar relationships hold for any one of the four different matrix elements. Our agenda included an empirical verification of these ratios. To this end polished aluminum plates of square shape with an edge length of 4 cm and a thickness of 0.5 cm were sandblasted with a mixture of glass beads of varying radii, ranging from 25 to 250 μm. The aluminum plates were bombarded with the glass beads at 10 psi. The sandblasted aluminum plates had to satisfy two criteria to qualify as targets with small scale roughness characteristics, as described in the following paragraph.

A surface with small scale roughness has its specular reflection coefficient modified according to the Davies formulas:

$$R_{HH}^r = R_{HH}(\theta_i)e^{-2(\frac{2\pi}{\lambda})^2 h^2\cos^2(\theta_i)} \tag{6}$$

$$R_{VV}^r = R_{VV}(\theta_i)e^{-2(\frac{2\pi}{\lambda})^2 h^2\cos^2(\theta_i)} \tag{7}$$

where the superscript r stands for "rough surface". R is the reflection coefficient that would be measured from a similar smooth surface. λ is the wavelength of the incident radiation and h^2 is the rms depth of the random surface. θ_i denotes the incident angle. Sandblasted samples were irradiated at several incident angles and the measured specular reflection coefficients were plotted as a function of $\cos^2\theta_i$. Samples that didn't satisfy the conditions imposed by the Davies formula, i.e. that $\frac{2\pi h}{\lambda} < 1$, were discarded. Samples that fit equations (6) and (7) were profiled by a mechanical profilometer. The profilometer output are traces of the surface profile along a straight line. These traces were visually inspected to check whether the rms depth, h^2, conformed with the corresponding numbers obtained from fitting the specular reflection coefficients to the Davies formula. The profilometer traces also provide information on the correlation length l. The Rice theory requires that the slopes be small and this too was established by the profilometeric measurement.

Section II which follows is devoted to a brief description of the experimental set-up. Section III contains graphical data for a variety of measurements. Section IV is devoted to a discussion of the data and its implications with respect to Rice theory.

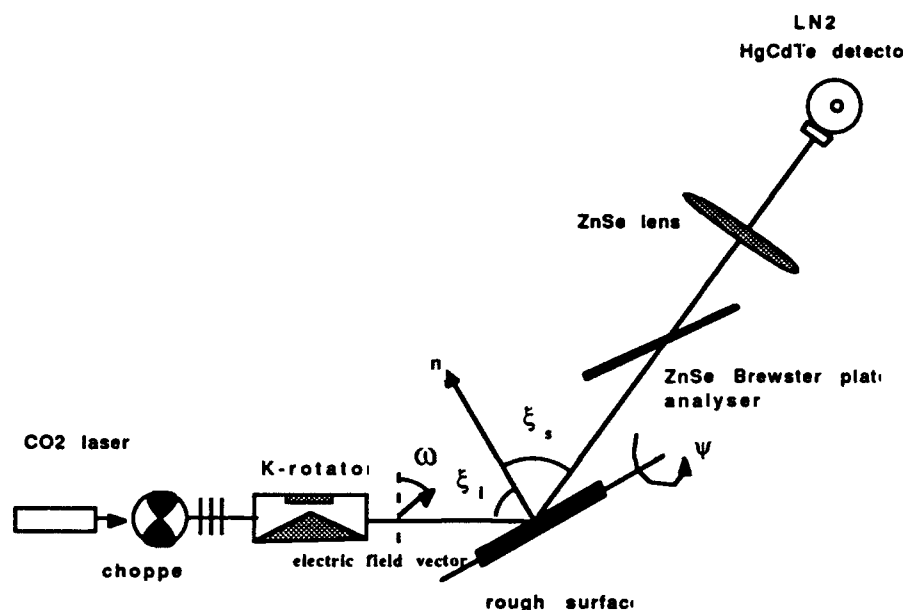## II. EXPERIMENTAL SETUP AND DISCUSSION OF LABORATORY ANGLES

Figure 1 Component Diagram of Scatterometer System

The source of radiation is a CO_2 laser (Ultra Lasertech Model 5122) providing 10 watts of linearly polarized radiation with a choice of 48 lines between 9.2 to 10.8 microns. The ability to rotate the linearly polarized radiation to any desired angle is provided by a K-rotator. The rough surface is allowed to rotate through two degrees of freedom which, in conjunction with the position of the detector, simulates the environment of a bistatic radar in the field (the relationship between field and lab coordinates is provided in the following paragraphs). At the receive end, discrimination between polarization states is accomplished by rotating a Brewster plate analyzer and wire grid polarizer analyzer. The combination of the two yields an extinction ratio of better than $1000 : 1$. The radiation is collected by a two inch diameter ZnSe lens with a focal length of 20 inches. A liquid nitrogen cooled HgCdTe detector (detectivity = 10^{10} cm $Hz^{1/2}$/Watt), mounted on a rotatable detector arm in the focal plane of the lens, scans the resultant intensity pattern. Scanning over a finite angular spread and averaging the data is necessitated by the scintillation pattern that results from the narrow-band laser radiation scattering from the rough surface. The detector output is fed to a lock-in amplifier and the time-averaged signal displayed on a Mac II computer.

The rough surface is mounted on a goniometer which can rotate through a range of $90°$. This rotation is about an axis that is parallel to a horizontal surface. The goniometer is mounted on a turn-

table which rotates through a vertical axis. By means of these two components, the target surface can be rotated around two axes.

The detector has a range of 270° and is rotated independently of the target surface.

The setup can simulate the three independent field angles, i.e., the incident and scattering polar angles from 0 to 90 °, and the scattering azimuthal angle from 0 to 180°. The rest of the azimuthal range, 180-360°, can be obtained by rotating the target surface around its mean normal.

The transformation of the field angles into the corresponding laboratory angles will now be derived.

In the field frame, the target surface orientation is fixed and the transmit and receive directions (vectors) can vary independently over a hemisphere (see Figure 2). In this frame, we designate the following angles θ_i, θ_s, and ϕ_s. θ_i stands for the incident angle, the angle between the incident propagation direction and target normal.

$$\mathbf{r}_i \cdot \mathbf{n} = -Cos(\theta_i) \tag{8}$$

where $\mathbf{r}_i$ is a unit vector along the direction of propagation, and $\mathbf{n}$ is a unit vector along the surface normal. Similarly,

$$\mathbf{r}_s \cdot \mathbf{n} = Cos(\theta_s) \tag{9}$$

where $\mathbf{r}_s$ is a unit vector along the detector direction and

$$\frac{[\mathbf{r}_i - \mathbf{n}(\mathbf{r}_i \cdot \mathbf{n})]}{Sin(\theta_i)} \cdot \frac{[\mathbf{r}_s - \mathbf{n}(\mathbf{r}_s \cdot \mathbf{n})]}{Sin(\theta_s)} = Cos(\phi_s) \tag{10}$$
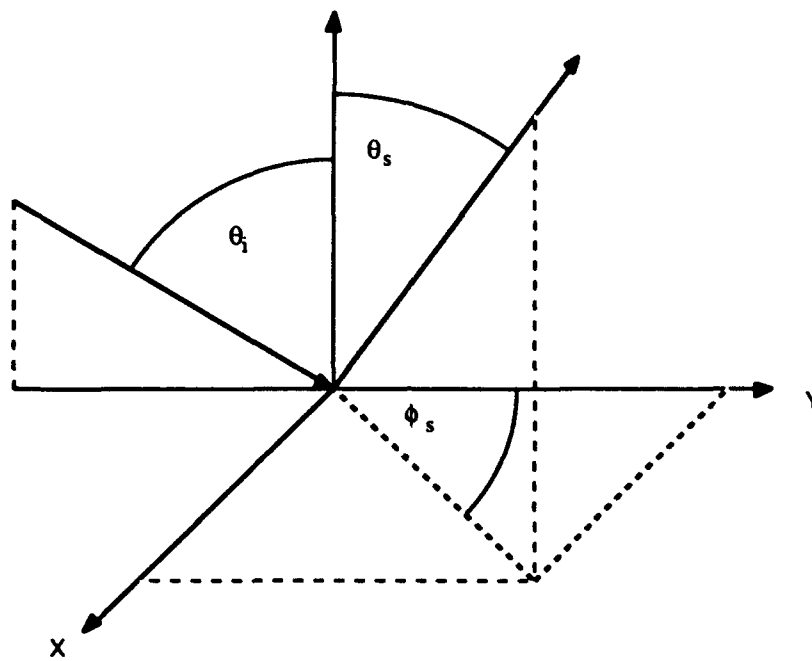
Figure 2. Definition of field angles
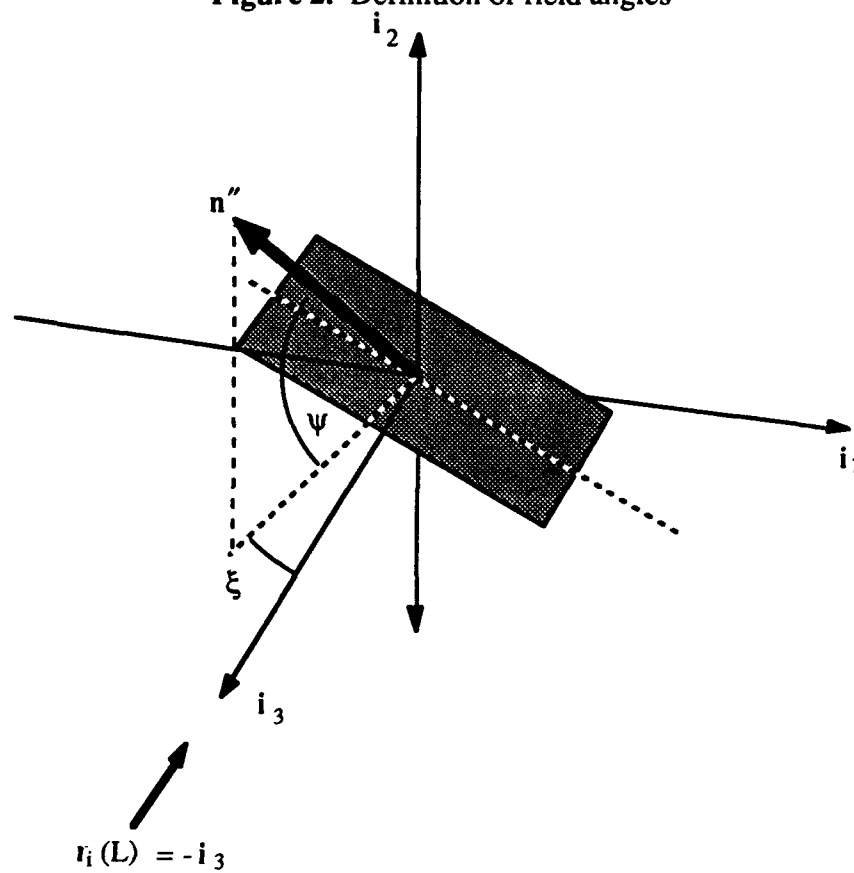
Figure 3. Definition of laboratory angles for $\xi \neq 0$ and $\psi \neq 0$

- 8 -
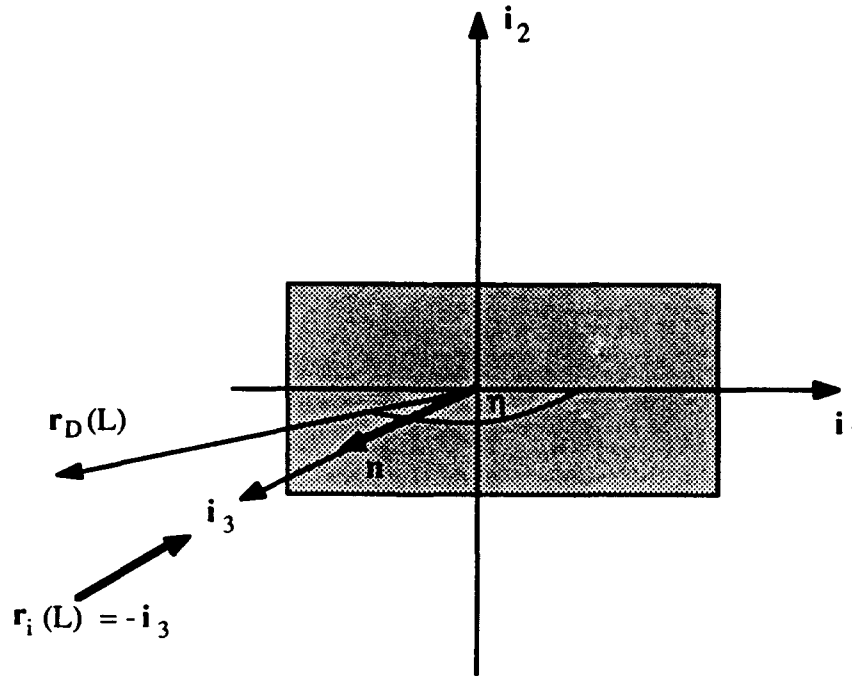
In the laboratory frame (Figure 3), the propagation direction is fixed, which is taken along the negative z-axis. Thus,

$$r_i(L) = -i_3 \qquad (11)$$

where L designates the laboratory frame and i_3 is a unit vector along the z-axis (Figure 3). The detector arm is in the x-z plane and can be rotated through 270° (Figure 4).

Hence

$$r_D(L) = Cos(\eta)\, i_1 + Sin(\eta)\, i_3 \qquad (12)$$

Figure 4. Laboratory system for $\psi = 0$ and $\xi = 0$ showing the detector position $r_D(L)$

The target surface normal can be rotated around two perpendicular axes. One rotation is around the y-axis (Figure 4), the axis perpendicular to the x-z plane containing the transmitter and receiver. The angle describing this rotation is designated by ξ. The range of ξ is 0° to 90°. The detector arm requires a 180° range for any fixed ξ. Hence, the full range of the detector has to be 270°.

A second rotation can be performed around the line which is the intersection of the target plane and the x-z plane (Figure 3).

The first rotation fixes ξ and the second rotation fixes ψ. When the target surface is rotated through ξ and ψ in succession, the normal to the target surface, expressed in the unit vectors of the laboratory coordinate system is:

$$\mathbf{n}'' = -\mathbf{i}_1 \, \text{Sin}(\xi) \, \text{Cos}(\psi) + \mathbf{i}_2 \, \text{Sin}(\psi) + \mathbf{i}_3 \, \text{Cos}(\xi) \, \text{Cos}(\psi) \tag{13}$$
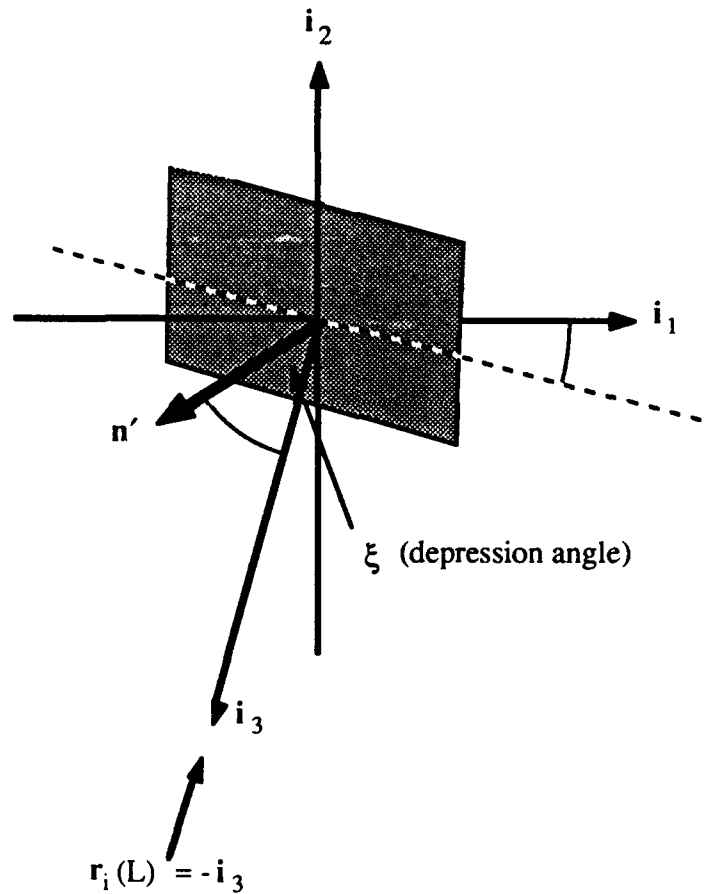
Figure 5. Laboratory system for $\xi \neq 0$ and $\psi = 0$

We note that the scalar products (1)-(3) defining the various field angles retain the same form when $\mathbf{n}''$ is substituted for $\mathbf{n}$. The following expressions relate laboratory angles (ξ, ψ, η) to field angles $(\theta_i, \theta_s, \phi_s)$.

$$Cos(\theta_i) = -\mathbf{r}_i \cdot \mathbf{n}'' = Cos(\xi)\,Cos(\psi) \qquad (14)$$

$$Cos(\theta_s) = \mathbf{r}_D \cdot \mathbf{n}'' = Sin(\eta - \xi)\,Cos(\psi) \qquad (15)$$

and

$$Cos(\phi_s) = \frac{\mathbf{r}_i \cdot \mathbf{r}_D - (\mathbf{r}_i \cdot \mathbf{n}'')(\mathbf{r}_D \cdot \mathbf{n}'')}{\sqrt{1 - (\mathbf{r}_i \cdot \mathbf{n}'')^2}\,\sqrt{1 - (\mathbf{r}_D \cdot \mathbf{n}'')^2}} \qquad (16)$$

substituting Eqns. (11),(12),(14) and (15) into Eqn. (16) yields:

$$Cos(\phi_s) = \frac{-Sin(\eta) + Cos^2(\psi)\,Sin(\xi - \eta)\,Cos(\xi)}{\sqrt{1 - Cos^2(\xi)\,Cos^2(\psi)}\,\sqrt{1 - Cos^2(\psi)\,Sin^2(\xi - \eta)}} \qquad (17)$$

We proceed to show that for a fixed θ_i and θ_s both larger than 0° (0° is a point of degeneracy) $Cos(\phi_s)$ can assume all values between -1 and +1. Denoting $Cos(\theta_i) = x$ and $Cos(\theta_s) = y$, equation (17) can be written as:

$$Cos(\phi_s) = \frac{-Sin(\eta) + yx}{\sqrt{1 - x^2}\,\sqrt{1 - y^2}} \qquad (18)$$

For a fixed ψ and ξ and a fixed y, η is not an independent variable. We therefore express $Sin(\eta)$ in terms of x, y, and ψ.

$$Sin(\eta) = Sin(\eta - \xi + \xi) = Sin(\eta - \xi)\,Cos(\xi) + Cos(\eta - \xi)\,Sin(\xi) \qquad (19)$$

or

$$Sin(\eta) = \frac{xy \pm [Cos^2(\psi) - y^2]\,[Cos^2(\psi) - x^2]}{Cos^2(\psi)} \qquad (20)$$

-11-

The minus sign in front of the square root has to be inserted when $(\eta - \xi) > 90°$. Combining (17)–(20) one writes:

$$\text{Cos}(\phi_s) = \frac{-xy\,\text{Tan}^2\psi \pm \sqrt{1 - \dfrac{y^2}{\text{Cos}^2\psi}}\ \sqrt{1 - \dfrac{x^2}{\text{Cos}^2\psi}}}{\sqrt{1 - y^2}\ \sqrt{1 - x^2}} \qquad (21)$$

We first show that $\text{Cos}(\phi_s)$ can assume the extreme values of ± 1. This can be seen by setting $\psi = 0$. The + sign in front of the square root yields +1, and the - sign yields -1. It is useful to rewrite the expression (14) as two equations each valid in a given range of $\text{Cos}(\phi_s)$. Assuming that $y > x$:

$$\text{Cos}(\phi_s) = \frac{-xy\,\text{Tan}^2\psi + \sqrt{1 - \dfrac{y^2}{\text{Cos}^2\psi}}\ \sqrt{1 - \dfrac{x^2}{\text{Cos}^2\psi}}}{\sqrt{1 - y^2}\ \sqrt{1 - x^2}} \qquad (22)$$

Eqn. (22) is valid for :

$$-\frac{x}{y}\sqrt{\frac{1 - y^2}{1 - x^2}} \le \text{Cos}(\phi_s) \le 1$$

and

$$\text{Cos}(\phi_s) = \frac{-xy\,\text{Tan}^2\psi - \sqrt{1 - \dfrac{y^2}{\text{Cos}^2\psi}}\ \sqrt{1 - \dfrac{x^2}{\text{Cos}^2\psi}}}{\sqrt{1 - y^2}\ \sqrt{1 - x^2}} \qquad (23)$$

Eqn. (23) is valid for :

$$-1 \le \text{Cos}(\phi_s) \le -\frac{x}{y}\sqrt{\frac{1 - y^2}{1 - x^2}}$$

For $x > y$, $-\dfrac{x}{y}\sqrt{\dfrac{1 - y^2}{1 - x^2}}$ must be replaced with $-\dfrac{y}{x}\sqrt{\dfrac{1 - x^2}{1 - y^2}}$. Since both functions are

continuous functions of ψ, for $0 \le \psi \le \text{Cos}^{-1}(y)$, $\text{Cos}(\phi_s)$ assumes all values in between.

The algorithm for determining ξ, η, ψ for a given θ_i, θ_s, ϕ_s is as follows. Compute $Cos(\phi_s)$ and select the larger of $Cos(\theta_s)$ or $Cos(\theta_i)$, thereby setting the appropriate range for equations (22) and (23). The value of $Cos(\phi_s)$ determines whether Eqn. (28) or (29) is to be used. Having selected the correct equation, one solves for $Cos(\psi)$ and determines ψ. Given $Cos(\psi)$, one then can determine $Cos(\xi)$ or ξ. η remains to be determined and is obtained from: $y = Cos(\theta_s) = Sin(\eta-\xi) Cos(\psi)$.

Since $Sin(\eta-\xi)$ is symmetric around $90°$, a unique determination of η depends on whether Eqn. (22) or (23) was used. For Eqn. (28), $\eta-\xi \geq 90°$ and for Eqn. (28) $\eta-\xi \leq 90°$.

To complete this section, we write down the direction of linear polarization that corresponds to an H transmit state. It is given by:

$$\mathbf{r}_i \times \mathbf{n}'' = -\mathbf{i}_1 Sin(\psi) + \mathbf{i}_2 Sin(\xi) Cos(\psi) \tag{24}$$

An H receive state is given by:

$$\mathbf{r}_D \times \mathbf{n}'' = -[\mathbf{i}_1 Sin(\eta) Cos(\xi) + \mathbf{i}_2 Cos(\eta-\xi)] Cos(\psi) + \mathbf{i}_3 Cos(\eta) Sin(\psi) \tag{25}$$

The V receive state is obtained from:

$$\mathbf{r}_D \times (\mathbf{r}_D \times \mathbf{n}'') = \mathbf{r}_D(\mathbf{r}_D \cdot \mathbf{n}'') - \mathbf{n}'' \tag{26}$$

or

$$\mathbf{r}_D \times (\mathbf{r}_D \times \mathbf{n}'') = \mathbf{i}_1 [Cos(\eta) Sin(\eta-\xi) + Sin(\xi)] Cos(\psi) + \mathbf{i}_2[Sin(\eta) Sin(\eta-\xi) \cdots \tag{27}$$

$$\cdots Cos(\psi) - Sin(\psi)] - \mathbf{i}_3 Cos(\xi) Cos(\psi) \tag{28}$$

III SCATTERING DATA

The data collected from targets with small scale roughness are represented graphically in this Section. Three different targets were used with rms facet depths of 0.44 µm , 0.51 µm, and 0.65 µm, respectively. The measurements include ratios of $\sigma_{VV} / \sigma_{HH}$ for $\phi_s = 0°$ and $180°$. For these azimuthal angles, the scattering plane coincides with the plane of incidence. Incident angles ranged from 10° to 50° degrees. Ratios of $\sigma_{HV} / \sigma_{VH}$ at an azimuthal angle of 90° and incident polar angles ranging from 10° to 50° are also presented.

Figures 6 - 10 , 19 - 23, and 32 - 36 represent in-plane scattering data.

The data are in reasonably good agreement with Rice theory in the forward direction, especially for the target with the smallest rms facet depth.

In the backward direction, i.e., with the azimuthal angle at 180°, the discrepancy between the theoretical prediction increases both with the scattering polar angle and with an increase of the rms facet depth. As an example, at an incident angle of 10° and scattering angles $\phi = 180°$, $\theta_s = 70°$, the predicted ratio of $\sigma_{VV} / \sigma_{HH}$ divided by the corresponding measured ratio ranges from 2.1 to 2.6. The larger discrepancy corresponds to a rms facet depth of 0.65 µm . These discrepancies get worse with incident polar angle. At an incident polar angle of 50°, similar discrepancies range from 4.5 to 5.2 with increasing rms facet depth. It is worth noting that these facet depths are still within the range of small scale roughness. The criteria for small scale roughness is that $\frac{2\pi h}{\lambda} < 1$. Even for h = 0.65 µm , $\frac{2\pi h}{\lambda} < 0.385$.

Figures 11-15, 24-28, and 37-41 display data on a log scale for $\sigma_{HV} / \sigma_{VH}$ ratios for the set of three small scale roughness surfaces and incident polar angles 10° to 50°. Although the data set follows the same trend as the calculated ratio, it can differ by as much of a factor of 3-4 from the

-14-

theoretical formula.

These discrepancies are quite surprising since the predicted ratios are independent of the exact nature of the correlation coefficients of the random rough surface. All that is required for agreement with the theory is that the first order perturbation calculations be valid. These requirements are that $\frac{2\pi h}{\lambda} < 1$, and that the slopes be small, i.e., $\frac{\partial z(x,y)}{\partial x} < 1$ and $\frac{\partial z(x,y)}{\partial y} < 1$. $z(x,y)$ is the height of the random surface at the point (x,y). Both the determination of the rms height through optical means, and profilometric traces of the rough surface, indicate that the small scale roughness criteria are satisfied.

The fabrication of surfaces that also possess Gaussian or exponential correlation coefficients is technically more demanding and was not attempted.

The theoretical prediction for the average incoherent scattering cross section per unit area is given by :

$$\gamma_{pq}^I = (\frac{4}{\pi} k_0^4 h^2 \cos^2\theta_i \cos^2\theta_s \, |\alpha_{pq}|^2) \; I \tag{29}$$

where I is given by one of the following forms.

$$I = \pi \, l^2 \exp[-k_0^2 \, l^2 \, (\xi_x^2 + \xi_y^2) / 4] \tag{30a}$$

$$I = 2 \, \pi \, l^2 \frac{1}{[\, 1 + k_0^2 \, l^2 \, (\xi_x^2 + \xi_y^2) \,]^{3/2}} \tag{30b}$$

Equation (30a) derives from integrating over a Gaussian correlation function for the random surface. Equation (30b) results from integrating over an exponential correlation function. It is interesting to note that for both Gaussian and exponential surface height correlation coefficients, the angular dependence of the scattering is identical, aside from the dependencies contained in I.

-15-

For both the Gaussian and exponential correlation functions, I depends on $(\xi_x{}^2 + \xi_y{}^2)$ where

$$\xi_y = \sin \theta_s \sin \phi_s \tag{30c}$$

$$\xi_x = \sin \theta_i - \sin \theta_s \cos \phi_s \tag{30d}$$

and

$$\xi_x{}^2 + \xi_y{}^2 = \sin^2\theta_i + \sin^2\theta_s - 2 \sin\theta_i \sin \theta_s \cos\phi_s \tag{30e}$$

Figures 16-18, 29-31, and 42-44, present data for various angular conditions, each obeying the constraint $\xi_x^2 + \xi_x^2 = 0.25$.

Thus for a fixed value of $(\xi_x{}^2 + \xi_y{}^2)$, the two factors of I are identical within a numerical factor. This motivated us to investigate a range of incident and scattering angles for which $(\xi_x{}^2 + \xi_y{}^2)$ is constant.

The results displayed in figures 16-18, 29-31, and 42-44 indicate that the surfaces failed to satisfy either Gaussian or exponential correlation functions.
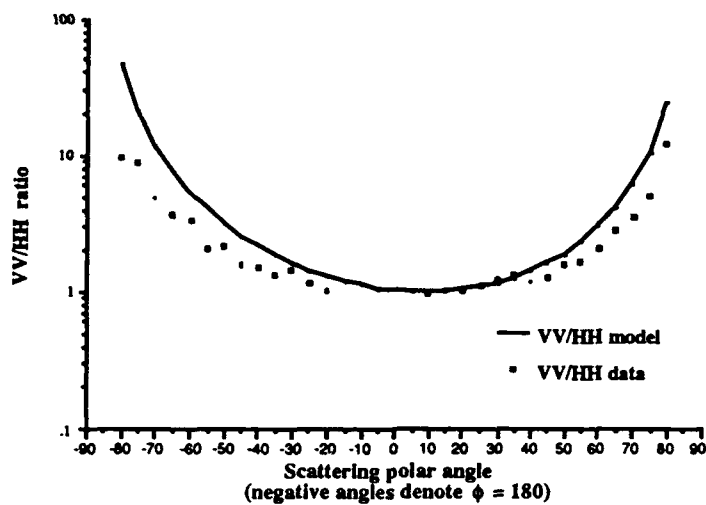
Figure 6

Scattering cross section ratio VV/HH : RMS facet Depth 0.44 μm,
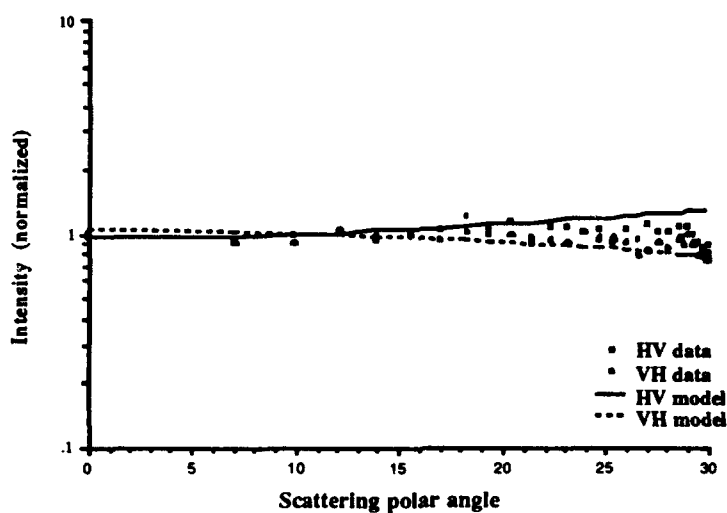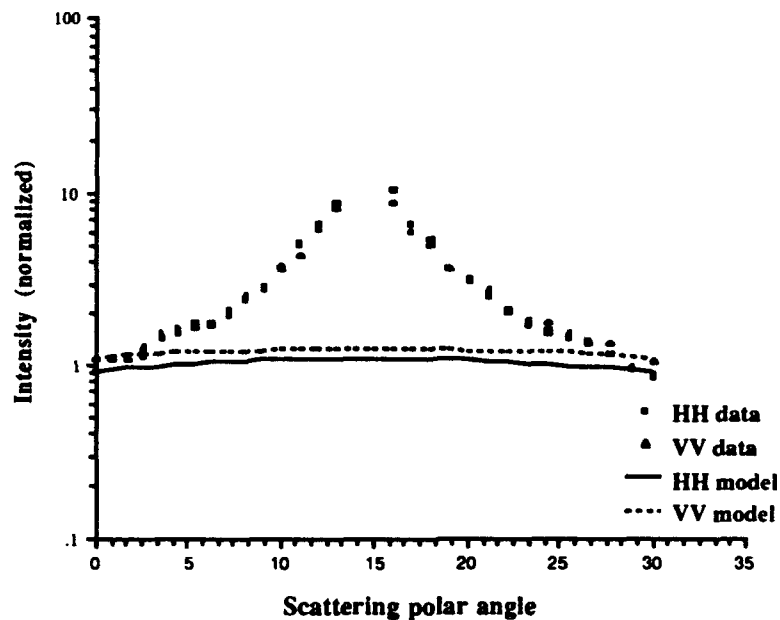Incident polar angle = 10 degrees, Azimuthal angle 0 - 180 degrees
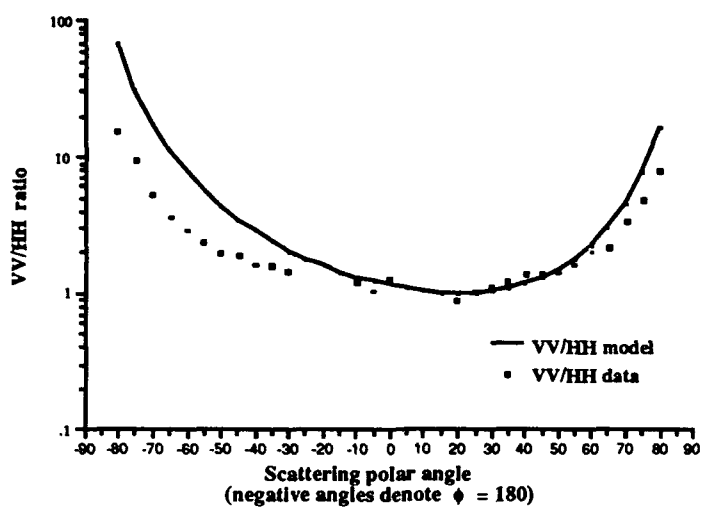
Figure 7

Scattering cross section ratio VV/HH : RMS facet Depth 0.44 μm,
Incident polar angle = 20 degrees, Azimuthal angle 0 - 180 degrees

-17-
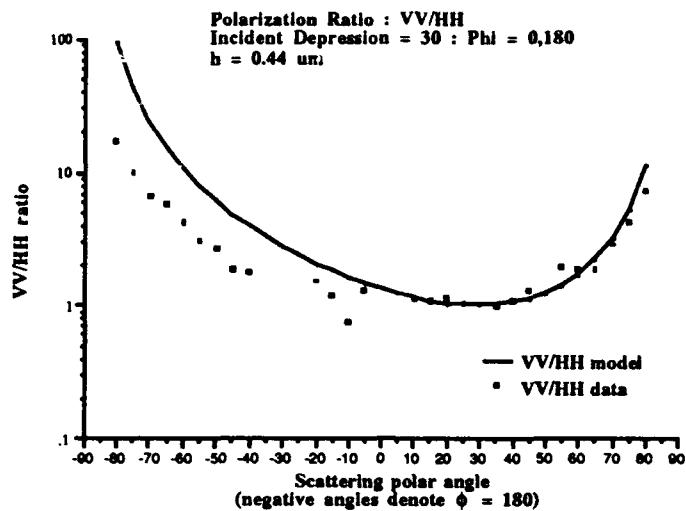
Figure 8

Scattering cross section ratio VV/HH : RMS facet Depth 0.44 μm,
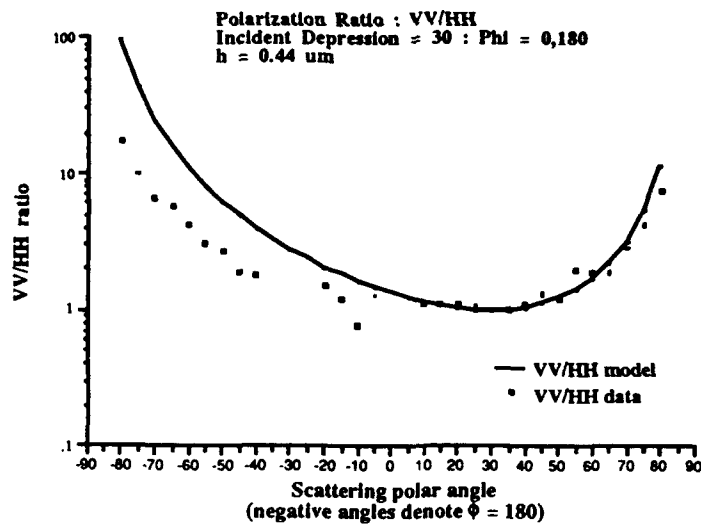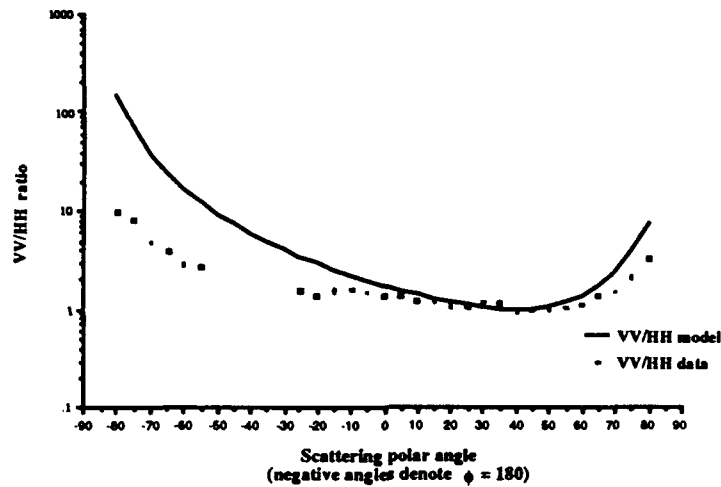Incident polar angle = 30 degrees, Azimuthal angle 0 - 180 degrees
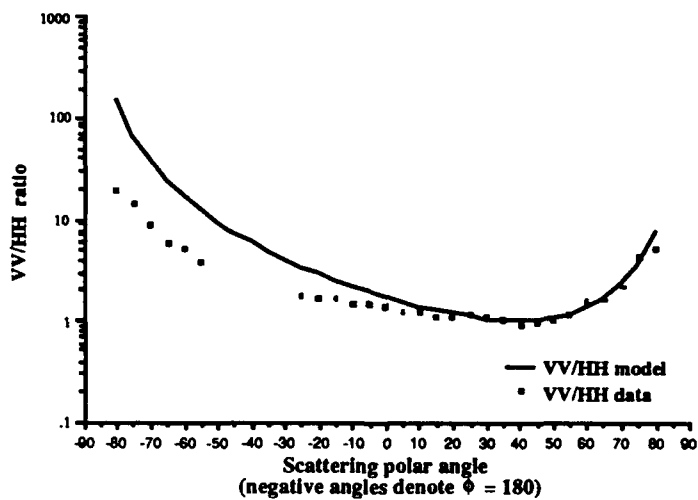
Figure 9

Scattering cross section ratio VV/HH : RMS facet Depth 0.44 μm,
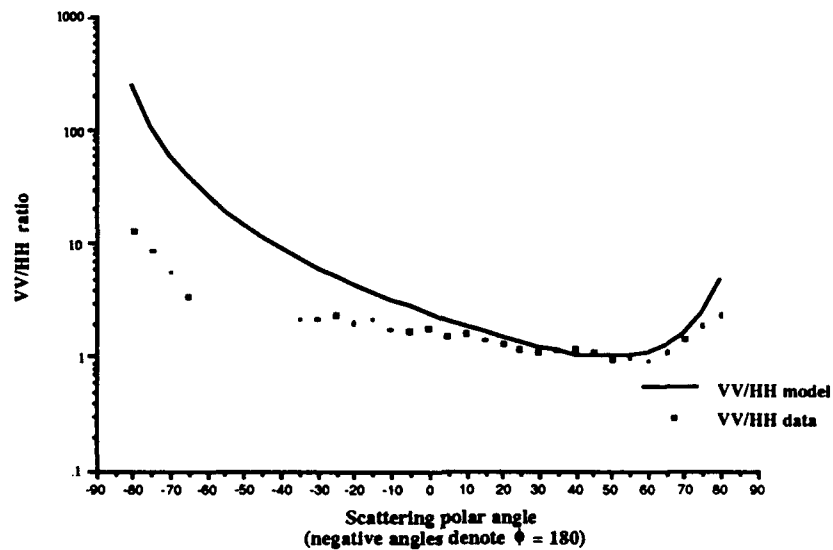Incident polar angle = 40 degrees, Azimuthal angle 0 - 180 degrees
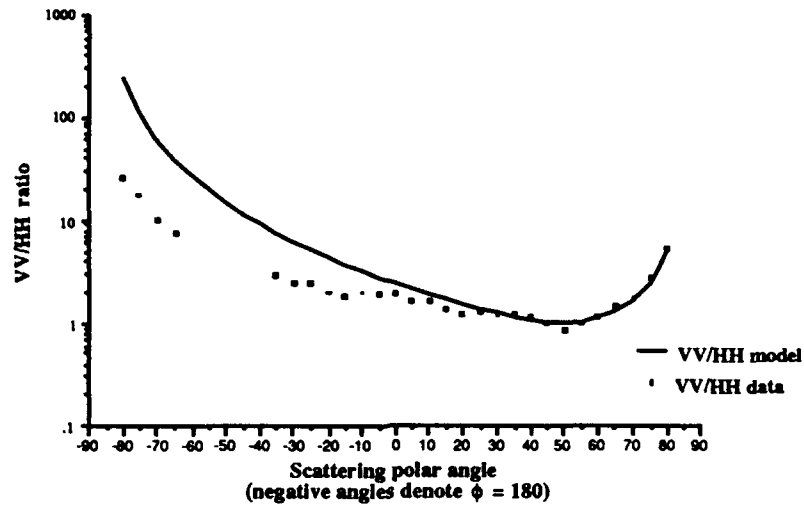
Figure 10
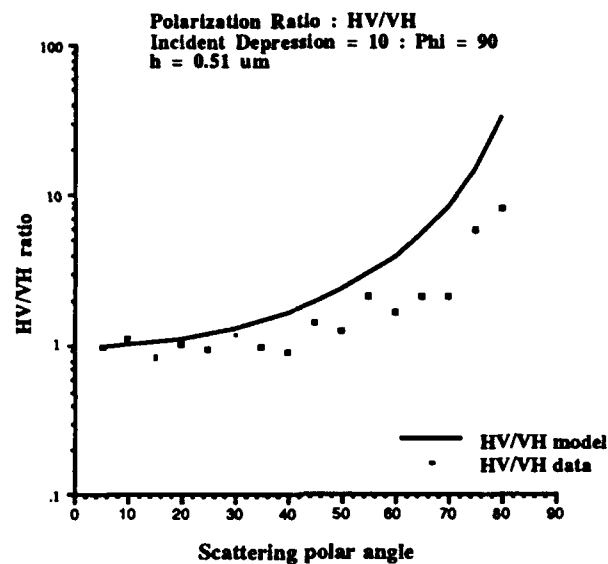
Scattering cross section ratio VV/HH : RMS facet Depth 0.44 μm,
Incident polar angle = 50 degrees, Azimuthal angle 0 - 180 degrees
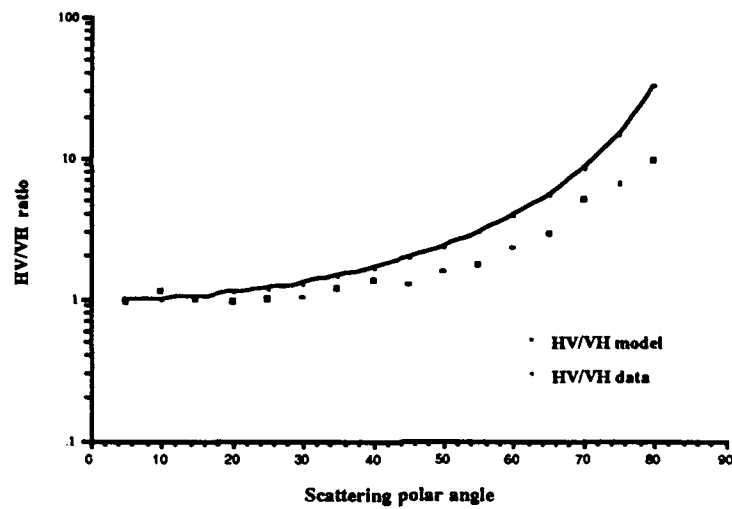
Figure 11

Scattering Cross Section ratio HV/VH : RMS facet Depth 0.44 μm,
Incident Polar Angle = 10 degrees, Azimuthal Angle 90 degrees
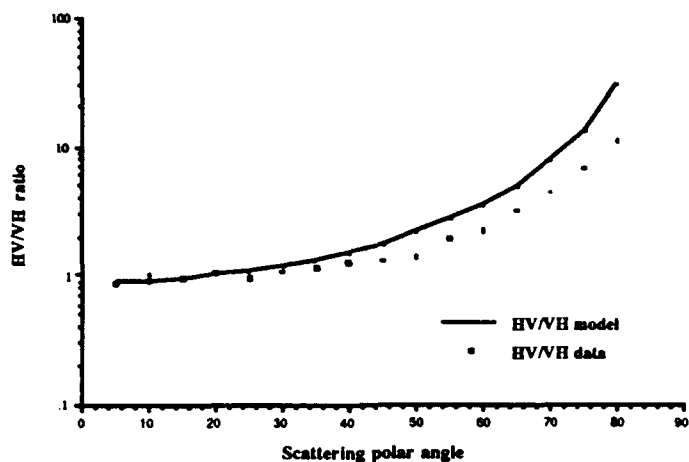
Figure 12

Scattering Cross Section ratio HV/VH : RMS facet Depth 0.44 μm,
Incident Polar Angle = 20 degrees, Azimuthal Angle 90 degrees
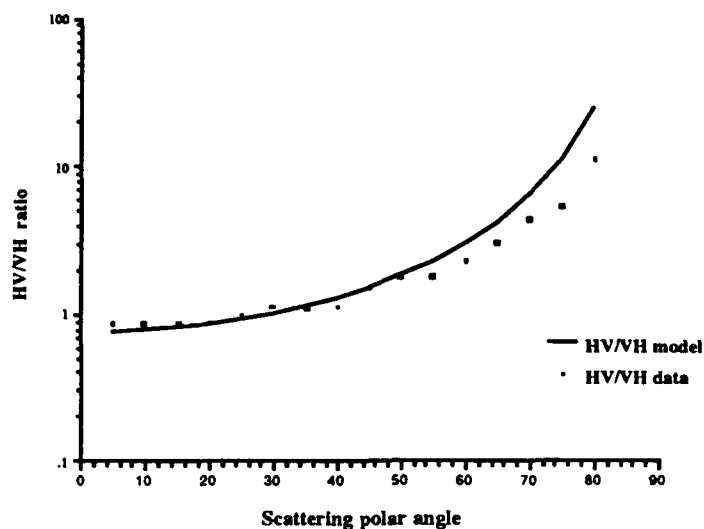
Figure 13

Scattering Cross Section ratio HV/VH : RMS facet Depth 0.44 μm,
Incident Polar Angle = 30 degrees, Azimuthal Angle 90 degrees
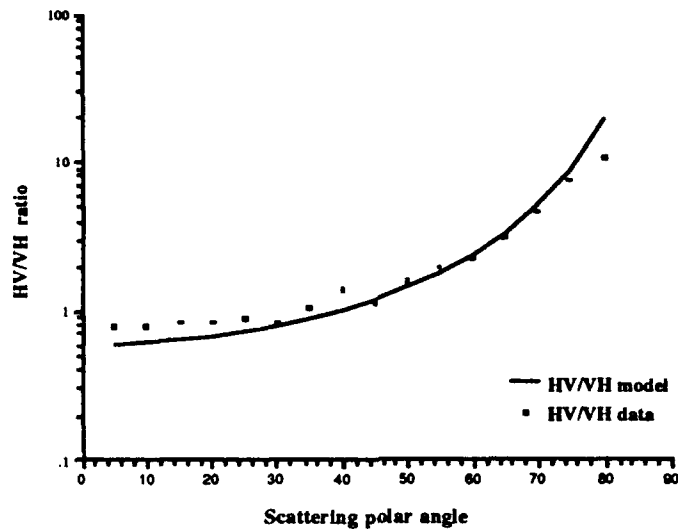
Figure 14

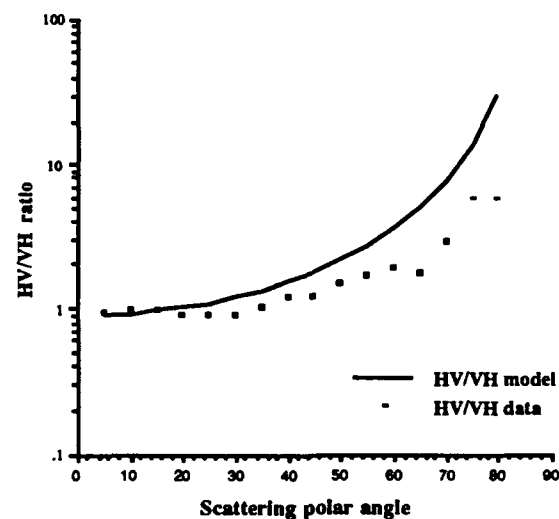**Scattering Cross Section ratio HV/VH : RMS facet Depth 0.44 μm,
Incident Polar Angle = 40 degrees, Azimuthal Angle 90 degrees**
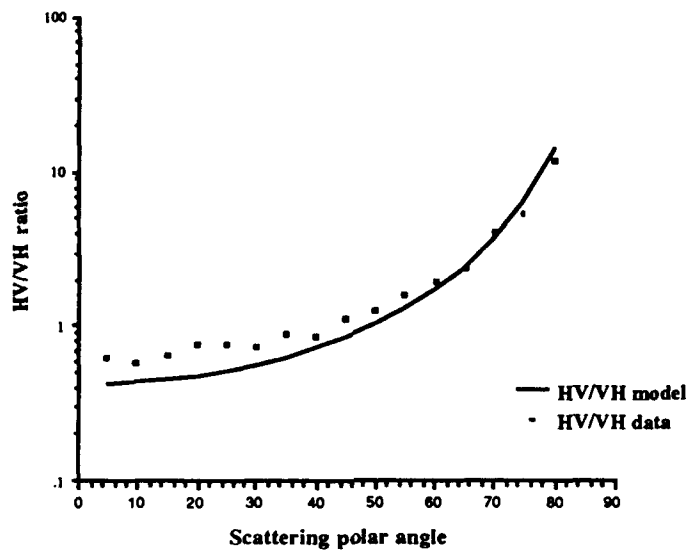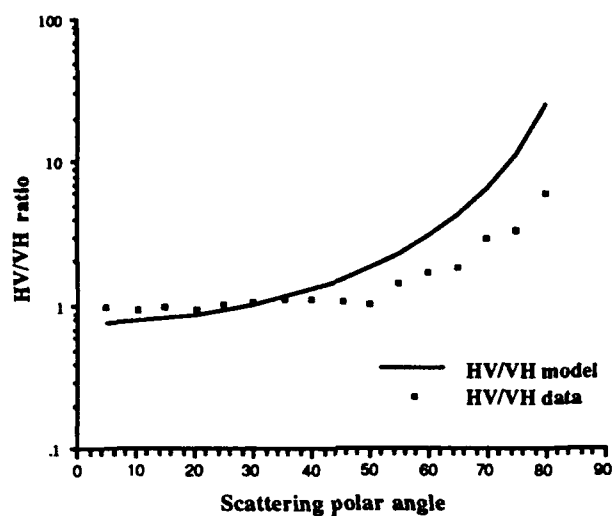

Figure 15

**Scattering Cross Section ratio HV/VH : RMS facet Depth 0.44 μm,
Incident Polar Angle = 50 degrees, Azimuthal Angle 90 degrees**
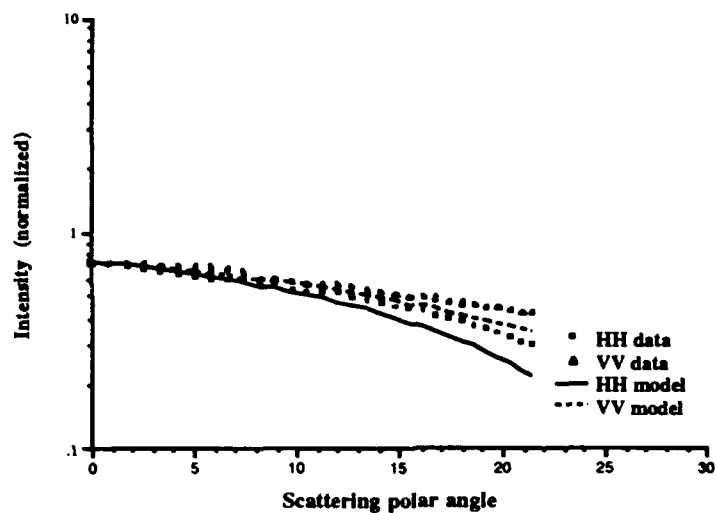
Figure 16

Co-Pol Scattering Cross Sections HH & VV : RMS facet Depth 0.44 μm,
Constraint condition = 0.25, Azimuthal Angle 0 degrees

Figure 17

Co-Pol Scattering Cross Sections HV & VH : RMS facet Depth 0.44 μm,
Constraint condition = 0.25, Azimuthal Angle 90 degrees

Figure 18

Co-Pol Scattering Cross Sections HH & VV : RMS facet Depth 0.44 μm,
Constraint condition = 0.25, Azimuthal Angle 180 degrees
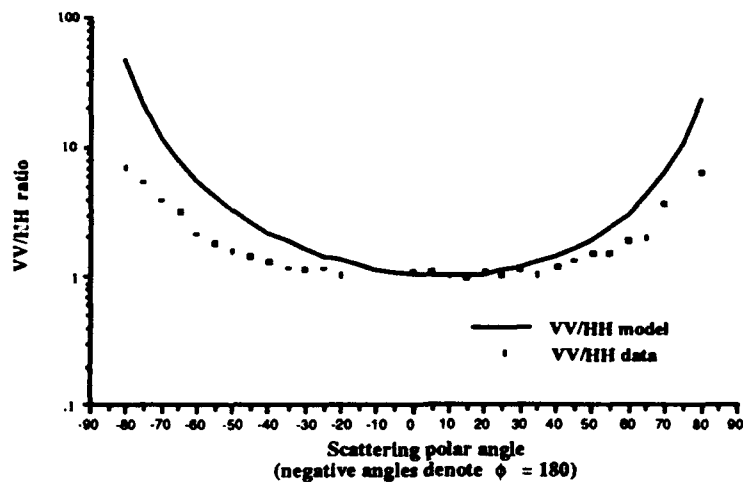
Figure 19

Scattering Cross Section ratio VV/HH : RMS facet Depth 0.51 μm,
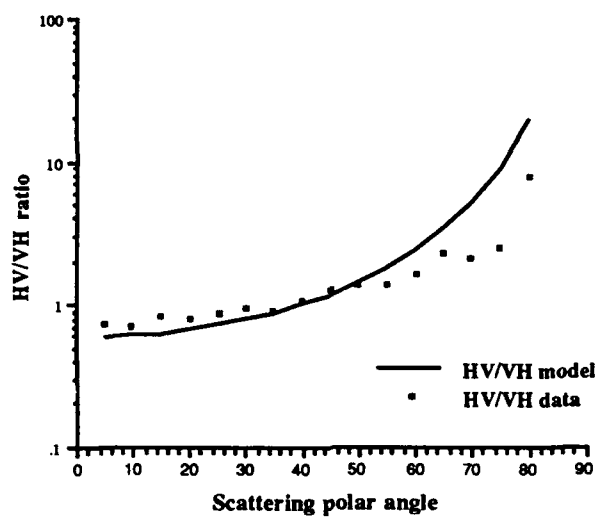Incident polar Angle = 10 degrees, Azimuthal Angle 0 - 180 degrees
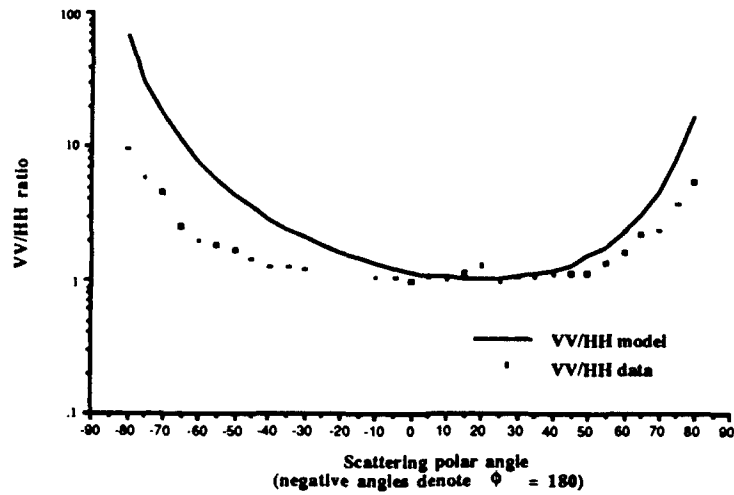
Figure 20

Scattering Cross Section ratio VV/HH : RMS facet Depth 0.51 μm,
Incident polar Angle = 20 degrees, Azimuthal Angle 0 - 180 degrees
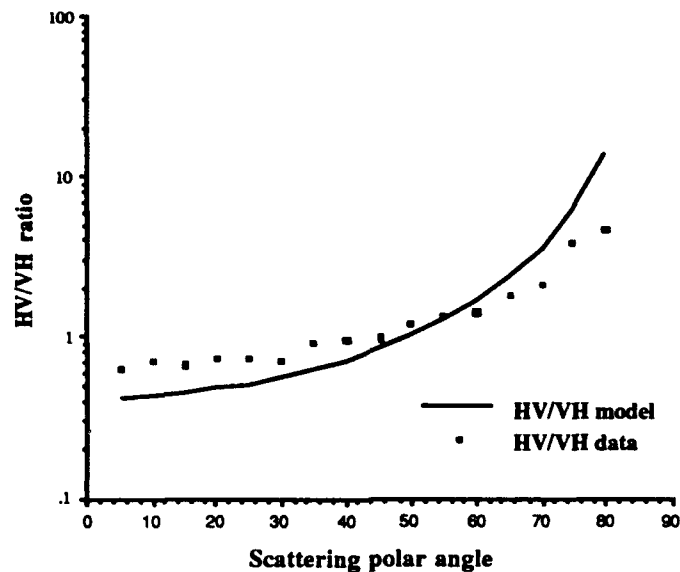

Figure 21

Scattering Cross Section ratio VV/HH : RMS facet Depth 0.51 μm,
Incident polar Angle = 30 degrees, Azimuthal Angle 0 - 180 degrees

Figure 22

Scattering Cross Section ratio VV/HH : RMS facet Depth 0.51 μm,
Incident polar Angle = 40 degrees, Azimuthal Angle 0 - 180 degrees

Figure 23

Scattering Cross Section ratio VV/HH : RMS facet Depth 0.51 μm,
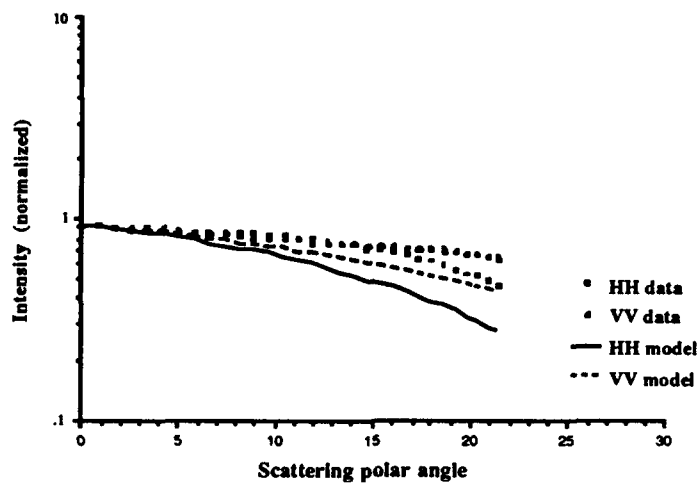Incident polar Angle = 50 degrees, Azimuthal Angle 0 - 180 degrees

Figure 24

Scattering Cross Section ratio HV/VH : RMS facet Depth 0.51 μm,
Incident Depression Angle = 10 degrees, Azimuthal Angle 90 degrees

Figure 25

Scattering Cross Section ratio HV/VH : RMS facet Depth 0.51 μm,
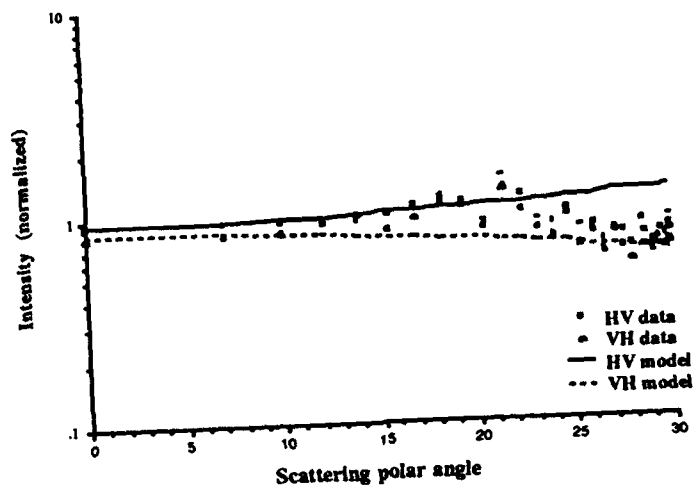Incident Depression Angle = 20 degrees, Azimuthal Angle 90 degrees

Figure 26

Scattering Cross Section ratio HV/VH : RMS facet Depth 0.51 μm,
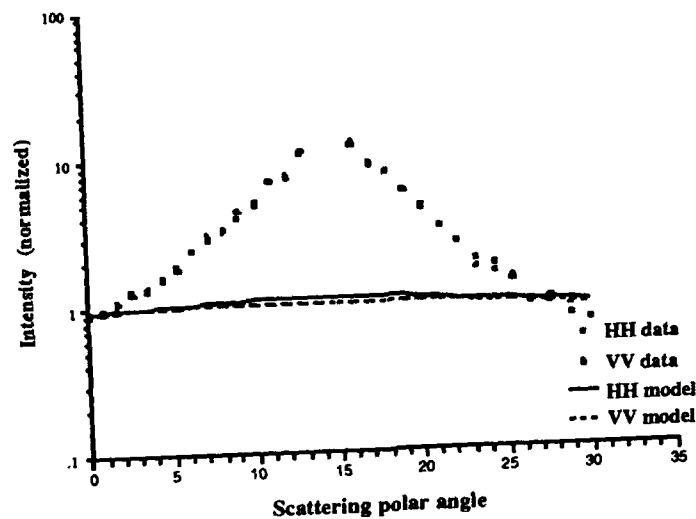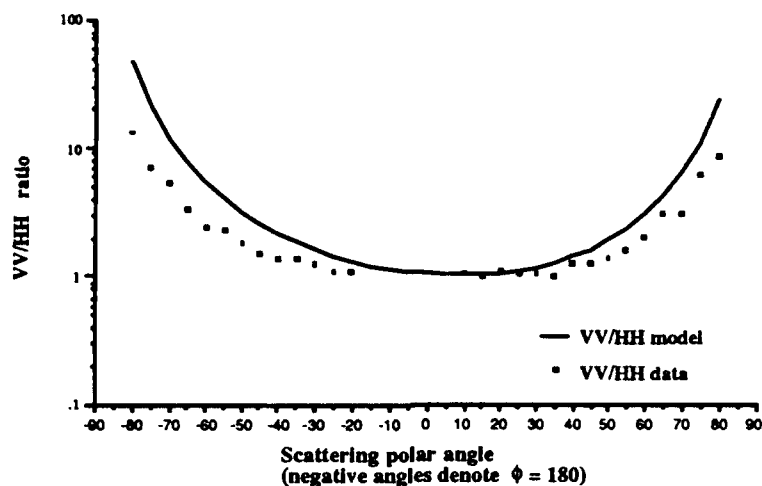Incident Depression Angle = 30 degrees, Azimuthal Angle 90 degrees

Figure 27

Scattering Cross Section ratio HV/VH : RMS facet Depth 0.51 μm,
Incident Depression Angle = 40 degrees, Azimuthal Angle 90 degrees

Figure 28

Scattering Cross Section ratio HV/VH : RMS facet Depth 0.51 μm,
Incident Depression Angle = 50 degrees, Azimuthal Angle 90 degrees

Figure 29

Co-Pol Scattering Cross Sections HH & VV : RMS facet Depth 0.51 μm,
Constraint condition = 0.25, Azimuthal Angle 0 degrees

Figure 30

Co-Pol Scattering Cross Sections HH & VV : RMS facet Depth 0.51 μm,
Constraint condition = 0.25, Azimuthal Angle 90 degrees

Figure 31

Co-Pol Scattering Cross Sections HH & VV : RMS facet Depth 0.51 μm,
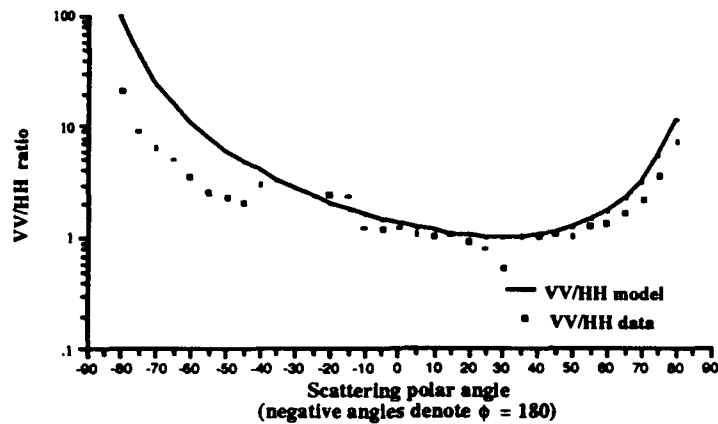Constraint condition = 0.25, Azimuthal Angle 180 degrees

Figure 32

Scattering Cross Section ratio VV/HH : RMS facet Depth 0.65 μm, Incident polar Angle = 10 degrees, Azimuthal Angle 0 - 180 degrees
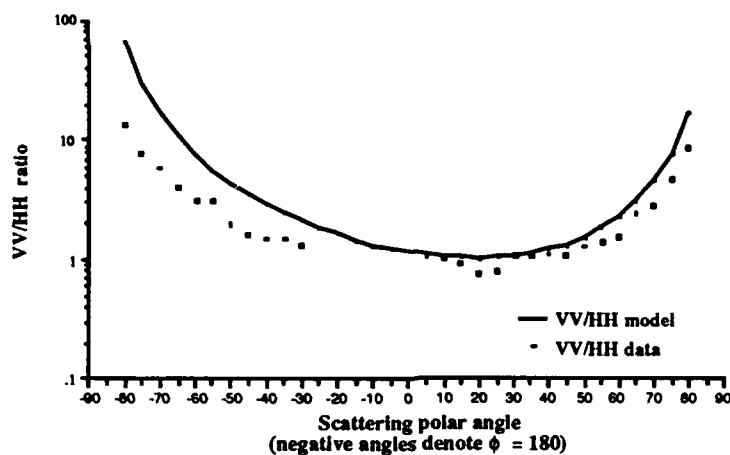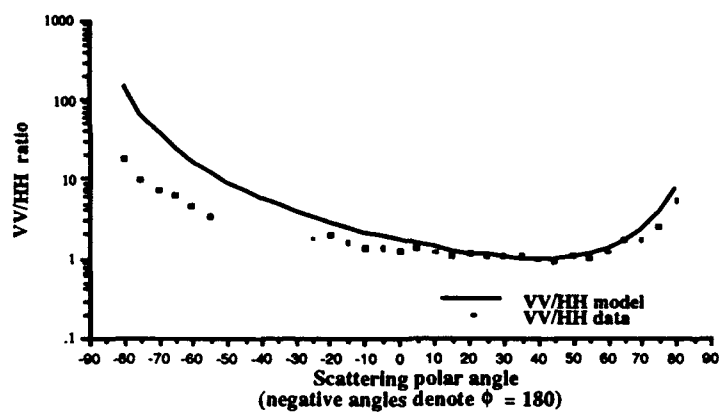

Figure 33

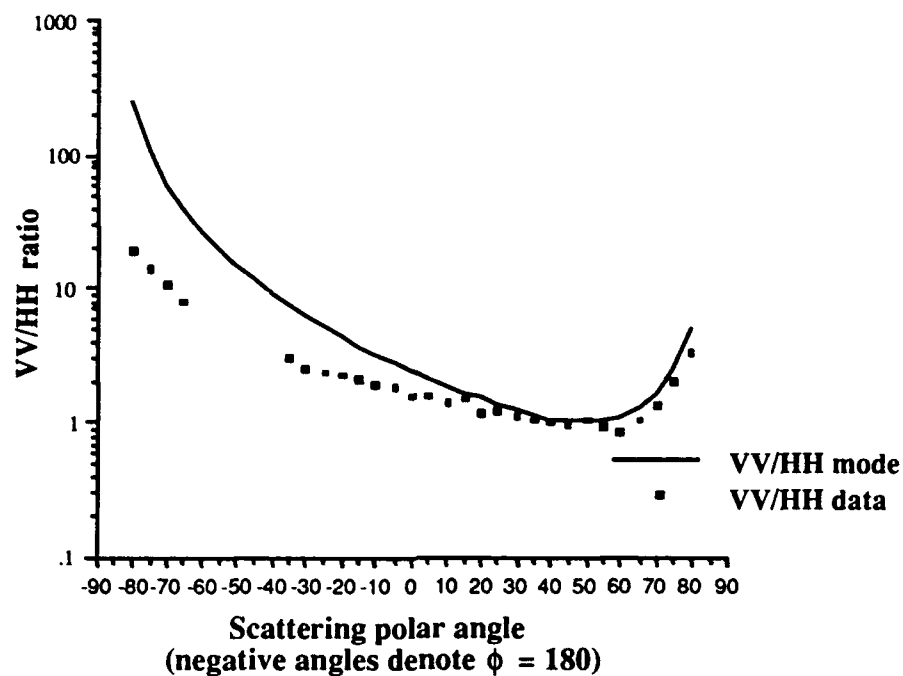Scattering Cross Section ratio VV/HH : RMS facet Depth 0.65 μm, Incident polar Angle = 20 degrees, Azimuthal Angle 0 - 180 degrees

Figure 34

Scattering Cross Section ratio VV/HH : RMS facet Depth 0.65 μm,
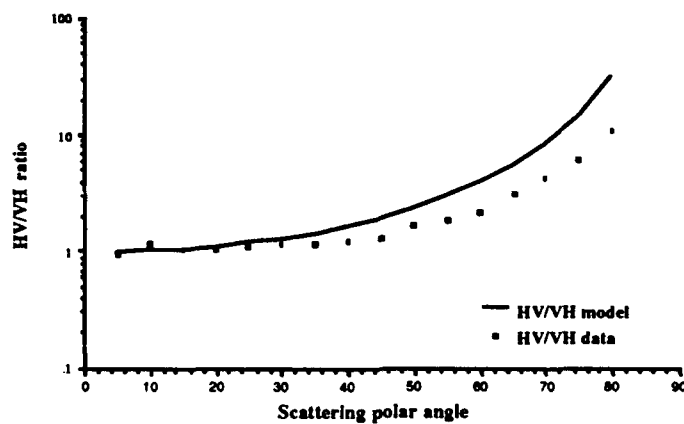Incident polar Angle = 30 degrees, Azimuthal Angle 0 - 180 degrees

Figure 35

Scattering Cross Section ratio VV/HH : RMS facet Depth 0.65 μm,
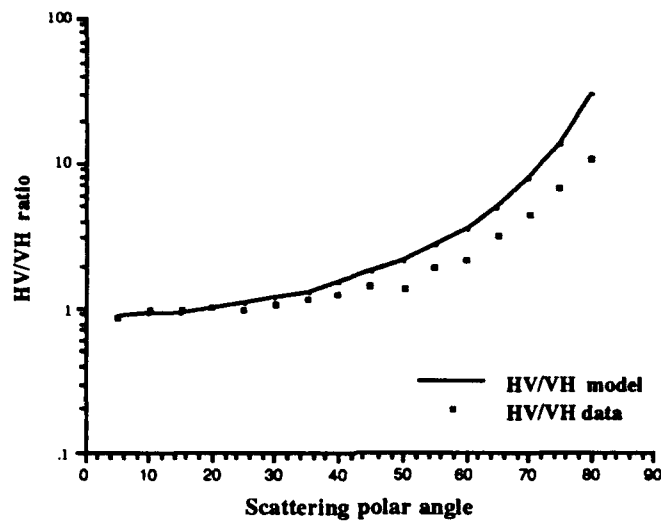Incident polar Angle = 40 degrees, Azimuthal Angle 0 - 180 degrees

Figure 36

Scattering Cross Section ratio VV/HH : RMS facet Depth 0.65 μm,
Incident polar Angle = 50 degrees, Azimuthal Angle 0 - 180 degrees

Figure 37

Scattering Cross Section ratio HV/VH : RMS facet Depth 0.65 μm,
Incident polar Angle = 10 degrees, Azimuthal Angle 90 degrees

Figure 38

Scattering Cross Section ratio HV/VH : RMS facet Depth 0.65 μm,
Incident polar Angle = 20 degrees, Azimuthal Angle 90 degrees
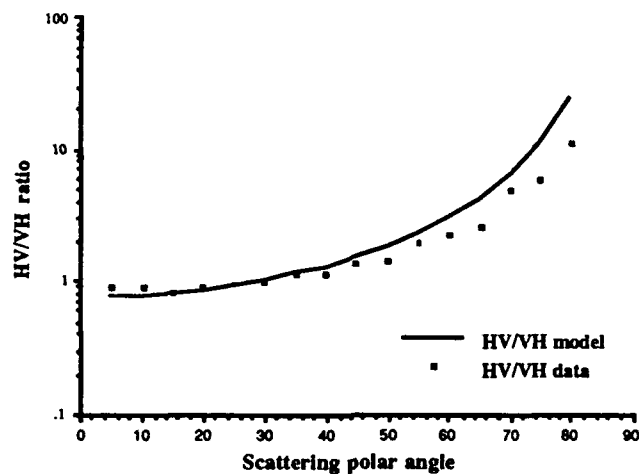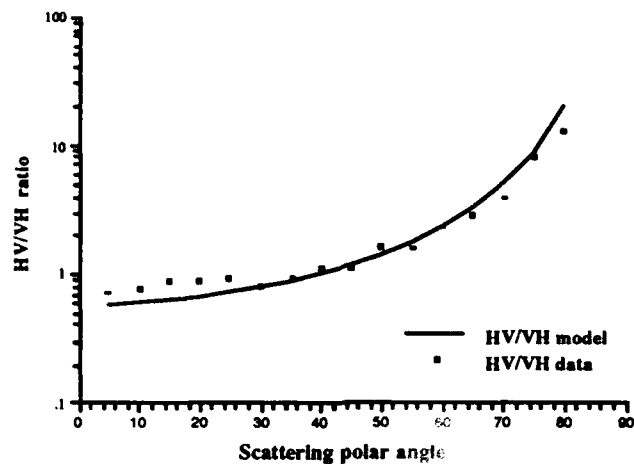

Figure 39

Scattering Cross Section ratio HV/VH : RMS facet Depth 0.65 μm,
Incident polar Angle = 30 degrees, Azimuthal Angle 90 degrees

Figure 40

Scattering Cross Section ratio HV/VH : RMS facet Depth 0.65 μm,
Incident polar Angle = 40 degrees, Azimuthal Angle 90 degrees
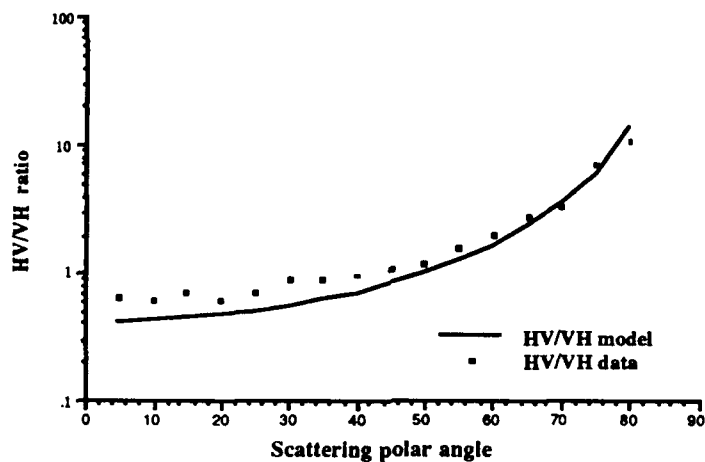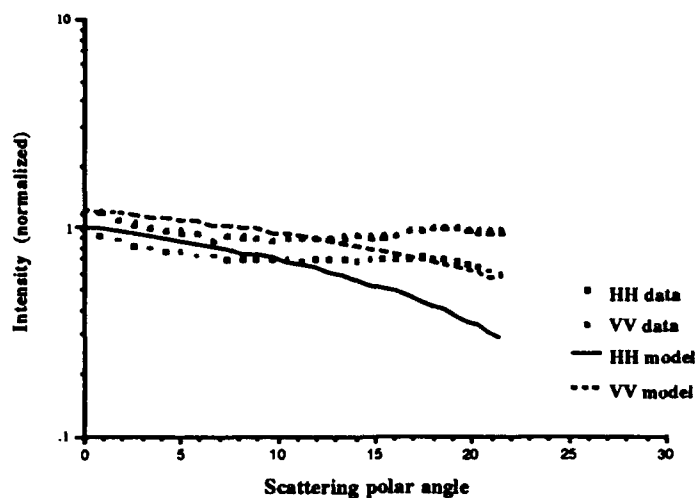

Figure 41

Scattering Cross Section ratio HV/VH : RMS facet Depth 0.65 μm,
Incident polar Angle = 50 degrees, Azimuthal Angle 90 degrees

Figure 42

Co-Pol Scattering Cross Sections HH & VV : RMS facet Depth 0.65 μm,
Constraint condition = 0.25, Azimuthal Angle 0 degrees
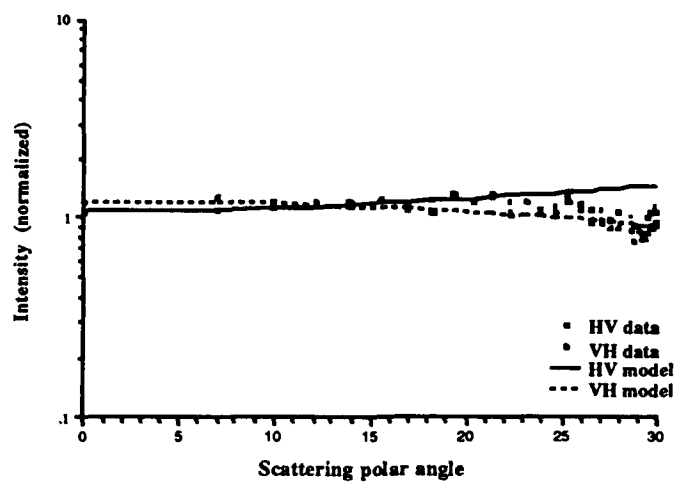
Figure 43

Co-Pol Scattering Cross Sections HH & VV : RMS facet Depth 0.65 μm,
Constraint condition = 0.25, Azimuthal Angle 90 degrees
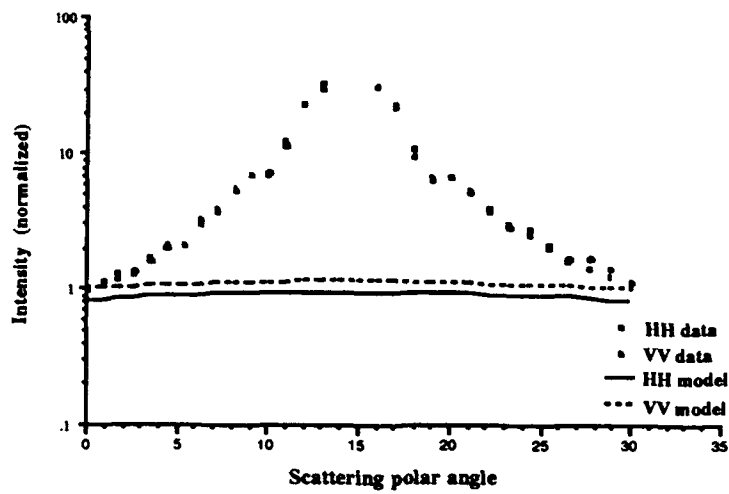
Figure 44

Co-Pol Scattering Cross Sections HH & VV : RMS facet Depth 0.65 μm,
Constraint condition = 0.25, Azimuthal Angle 180 degrees
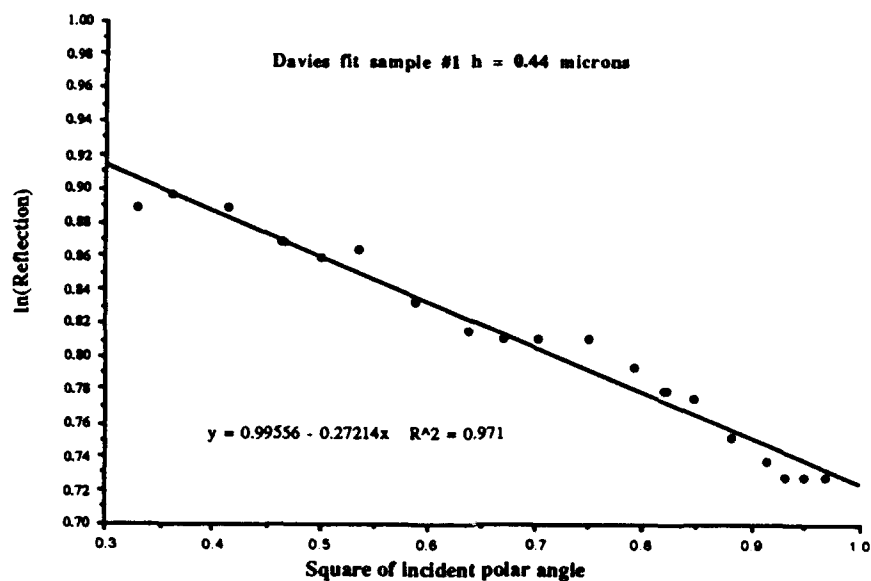
Figure 45
Surface roughness (facet depth) determined for Sample #1
h = 0.44 μm from best fit to Davies formula.
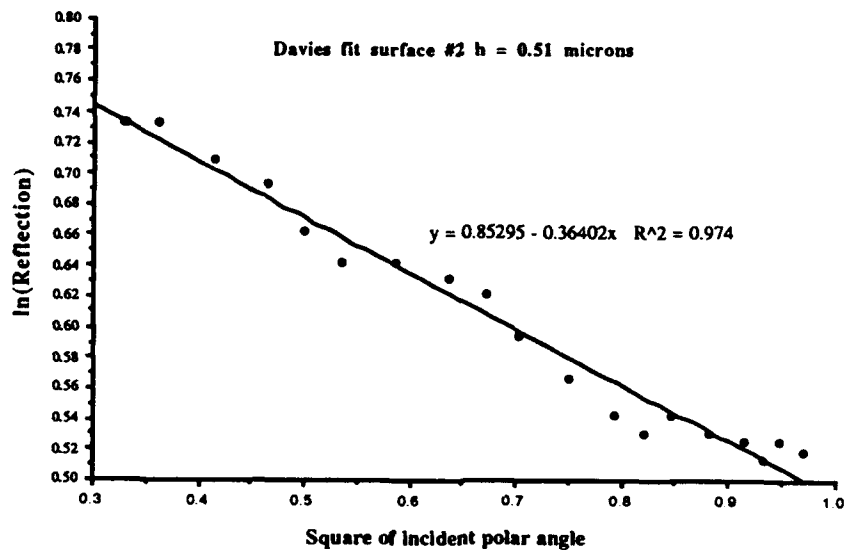
Figure 46
Surface roughness (facet depth) determined for Sample #2
h = 0.51 μm from best fit to Davies formula.
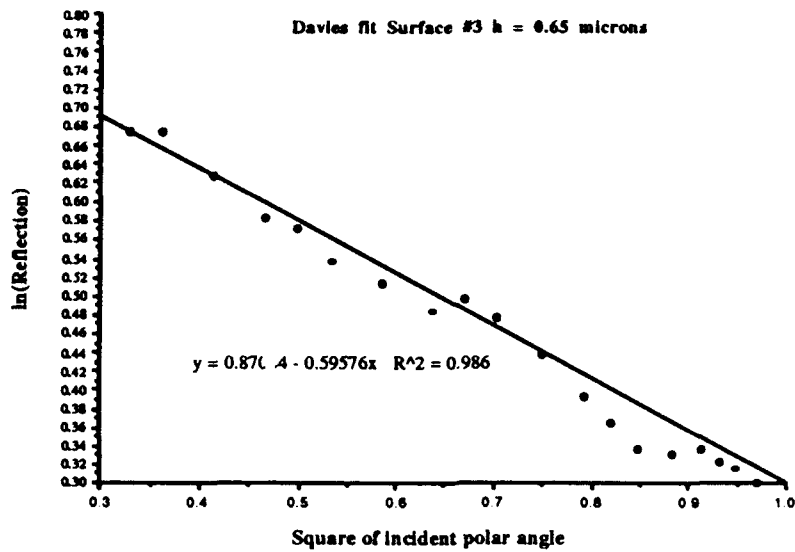
Figure 47
Surface roughness (facet depth) determined for Sample #3
h = 0.65 μm   from best fit to Davies formula.

IV Discussion of Results

The data presented, especially the ratios of cross section for diverse polarization states, leads us to conclude that first order perturbation theory is not valid.

Our measurements show that the criteria for the validity of first order perturbation theory are the characteristics of the target surfaces as described below. •

i) $\qquad \dfrac{2\pi h}{\lambda} < 1$

and

ii) $\qquad \dfrac{\partial z(x,y)}{\partial x} < 1$ and $\dfrac{\partial z(x,y)}{\partial y} < 1$

Equations i) and ii) contain the necessary constraints on the facet depths and slopes, respectively.

A third criterion that is required to derive a closed form expression for the scattering cross section for a small scale rough target is that the roughness is isotropic. As was pointed out, however, by D.E.Barick and W. H Peake[4], this requirement is not essential for a theoretical solution of the problem[5]. It is certainly not essential in making the following assertion. If first order perturbation theory is valid, then the predicted ratios of $\dfrac{\sigma_{VV}}{\sigma_{HH}}$ and $\dfrac{\sigma_{HV}}{\sigma_{VH}}$ should be in agreement with the data for small values of $(\dfrac{2\pi h}{\lambda})^2$. Any deviation from predicted results should be of the order of 10%. Our data indicate discrepancies as a high as a factor of 5. It is unlikely that the coefficient multiplying the expansion parameter $(\dfrac{2\pi h}{\lambda})^2$ would be a factor of 50.

The origin of the discrepancy may be due to the assumption that perturbation theory is valid. The validity of perturbation theory hinges on the absence of singularities in the exact result.

We present an heuristic argument that questions the validity of perturbation theory for

electromagnetic scattering from small scale rough surfaces. The argument is as follows.

Consider the case of an infinitely long thin wire. Since $\frac{2\pi h}{\lambda} < 1$, one would assume that a theoretical expansion in powers of $\frac{2\pi a}{\lambda}$ would be valid. This, however, is not the case for an electromagnetic wave incident on a thin conduction wire with the E field parallel to the wire. The scattering amplitude in the far zone is given below[6].

$$E_s'' = E_i'' \sqrt{\frac{\pi}{2}} \; \frac{1}{\sqrt{k_0 \cdot r}} \; \frac{e^{i(k \cdot r + \frac{\pi}{4})}}{\ln(0.895 \; k_0 a) \; -i\frac{\pi}{2}} \tag{31}$$

The exact result shows that for a thin wire with the incident electric field parallel to the cylinder axis, there is a logarithmic singularity, and therefore the expression cannot be expanded in a power series of $(k_0 a)$.

No such singularity exists for an incident electromagnetic wave with an electric field in the plane of incidence. A small scale rough surface fabricated with a random distribution of thin wires of varying radii and spacing on a flat substrate would satisfy the necessary requirements for the Rice Theory. Yet it is doubtful that the logarithmic singularity inherent in each isolated wire would vanish, as a result of the random distribution of the wire or of the multiple scattering from one wire to all others.

We conclude by stating that the data presented here are in disagreement with first order perturbation theoretical predictions. This disagreement may very well be due to the invalidity of perturbation theory.

As a consequence of these disappointing results, we considered it futile to investigate the validity of the theoretical predictions for a random surface with two scale roughness. Our previous

-40-

work on large scale rough surfaces demonstrated that the predictions of the facet model theory were not valid[8]. The fusion of these two theoretical models cannot overcome the inherent limitations of each.

REFERENCES / FOOTNOTES

[1]   Lord Rayleigh, Theory of Sound, Vol. 2, Macmillan, London, 1929, pp. 89 -96

[2]   Stephen O. Rice, "Reflection of Electromagnetic Waves from Slightly Rough Surfaces",
        Theory of Electromagnetic Waves, edited by Morris Kline, Dover Publications, N. Y., 1951

[3]   D. E. Barrick, "Rough Surfaces", Radar Cross Section Handbook, Vol. 2, edited by Ruck,
        Barrick, Stuart, Krichbaum, Plenum Press, New York - London, 1970, pp. 703 - 709

[4]   D. E. Barrick and W. H. Peake, "Scattering from Surfaces with different Roughness Scales:
        Analysis and Interpretation", Battelle Memorial Institute, Columbus, Ohio, BAT-197A-3

[5]   An additional requirement that the target must satisfy is that the square of the correlation length
        is smaller than the illuminated area. This requirement was easily satisfied by our target
        samples and the laser beam.

[6]   D. E. Barrick, "Rough Surfaces", Radar Cross Section Handbook, Vol. 1, edited by Ruck,
        Barrick, Stuart, Krichbaum, Vol. 1, Plenum Press, New York - London, 1970, pp. 211

[7]   ibid, pp. 704

[8]   Z. Fried, G. Phillips, J. Waldman, "Laboratory measurements of scattered electromagnetic
        radiation from two dimensional metallic and dielectric rough surfaces", J. Opt. Soc. Am.
        B, Vol.9, No.5, May 1992